Communications

Broadband Dual Linear Polarized Antenna for Statistical Detection of Breast Cancer

Douglas A. Woten and Magda El-Shenawee

***Abstract*—A broadband planar antenna capable of dual linear polarization is designed to be used for the detection of breast tumors. This antenna along with a breast model is simulated using the Ansoft HFSS v10.1. The S-parameters are used as input to Artificial Neural Networks for data processing to investigate the effect of polarization on the statistical detection. Using a dual polarized antenna allowed the calculation of all vertical and horizontal co- and cross-polarizations. The numerical results show that using polarizations parallel to the tumor's major axis increases the likelihood of tumor detection.**

***Index Terms*—Artificial neural network, breast cancer detection, broadband antenna.**

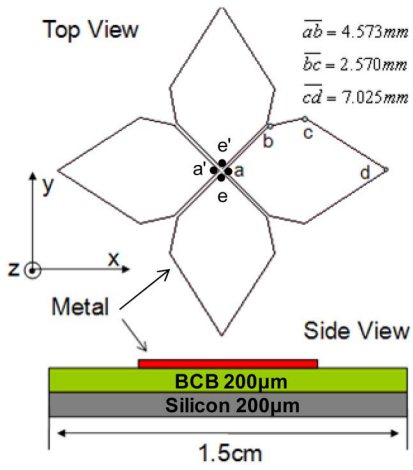

Fig. 1. Geometry of designed Fourtear antenna.

I. Introduction

The electrical properties of the breast and breast tumors have been the subject of much research. Originally, it was reported that a large contrast ($\sim 10-1$) existed between the electrical properties of the tumor and healthy breast tissue at 3.2 GHz [1]. Recent work, however, has reported that the contrast is on average as low as 10% when compared to the surrounding fibro-glandular tissue [2], [3]. It is possible, however, for a high contrast to exist in very fatty breasts containing 85%–100% adipose tissue [2]. This high fat content could be property of breasts which have undergone shrinking of the ducts and lobules associated with older women. The presented statistical detection scheme is believed to work better on these high contrast cases.

This work uses a variation of the high contrast numbers reported in [1], and explores the use of all polarizations to increase tumor detection rates based on artificial neural networks (ANNs). Due to the ANN's real-time results and intrinsic flexibility in configuration and adaptation, these networks are ideal as preprocessors to the more time intensive imaging algorithms [4]. A model utilizing the low contrast numbers and the breast skin is commented on in relation to the effects on statistical detection.

Broadband antennas are necessary to increase the possibility of detecting tumors over a large range of sizes. The Fourtear antenna is a planar broadband dual linearly polarized antenna [5] (Fig. 5.18 in this reference). The current work focuses on modifying this antenna and using the complex S-parameters for statistical detection. The size and weight of the original antenna are reduced to allow for future integration with a micro-electro-mechanical-systems (MEMS) rotatable platform.

Manuscript received July 29, 2007; revised April 19, 2008. Current version published November 14, 2008. This work was supported in part by the NSF Graduate Research Fellowship NSF GK-12 Program, NSF Award Number ECS-0524042, the Arkansas Biosciences Institute (ABI), and in part by the Women's Giving Circle at the University of Arkansas.

D. A. Woten is with the Microelectronics-Photonics Program (MicroEP), University of Arkansas, Fayetteville, AR 72701 USA (e-mail: dwoten@uark.edu)

M. El-Shenawee is with the Electrical Engineering Department, University of Arkansas, Fayetteville, AR 72701 USA (e-mail: magda@uark.edu).

Color versions of one or more of the figures in this paper are available online at http://ieeexplore.ieee.org.

Digital Object Identifier 10.1109/TAP.2008.2005545

II. Antenna Design

A. Fourtear Antenna

One advantage of this antenna is the ability to transmit and receive dual linear polarizations. The other advantage is its broad bandwidth of operation, 2–10 GHz as reported in [5]. The design presented in [5] used a substrate of 16.51×16.51 cm^2 with a ground plane placed at 3.81 centimeters below the substrate separated by foam. The substrate is 0.079 cm thick and made of Rogers Duroid 5870 with $\varepsilon_r = 2.33$. The overall height of the antenna was 4.6 cm [5]. The antenna is fed using a coaxial line with the feed points separated by 0.356 cm.

In this work, two layers of substrate materials of silicon and benzocyclobutene (BCB) respectively are used to replace the Rogers Duroid 5870 in [5]. Each layer is limited to 0.02 cm in order to reduce the overall substrate thickness to 0.04 cm compared to 4.6 cm in [5]. The overall size of the substrate is also constrained to 1.5×1.5 cm^2 compared to 16.51×16.51 cm^2 in [5]. The original antenna in [5] had different shaped arms to improve the bandwidth, while in this work identical arms are used to ensure identical excitation for both polarizations. A two wire feed line is used between a'a or e'e at a distance of 0.36 cm. Using these design considerations, the prototype antenna is shown in Fig. 1 and is simulated using the Ansoft High Frequency Structure Simulator (HFSS) v10.1.

B. Antenna Performance

The simulated antenna impedance and reactance is shown in Fig. 2(a). This figure shows that the impedance varies closely around 50-Ω while the reactance is near 0-Ω in the antenna's resonant frequency band. This result agrees with a linear gap antenna shown in Figure 5-3 in [5]. The S_{11} (referenced to 50-Ω) for the antenna in air is calculated using the HFSS and is shown in Fig. 2(b). The bandwidth of the antenna is 67% using a center frequency of 7.5 GHz and it

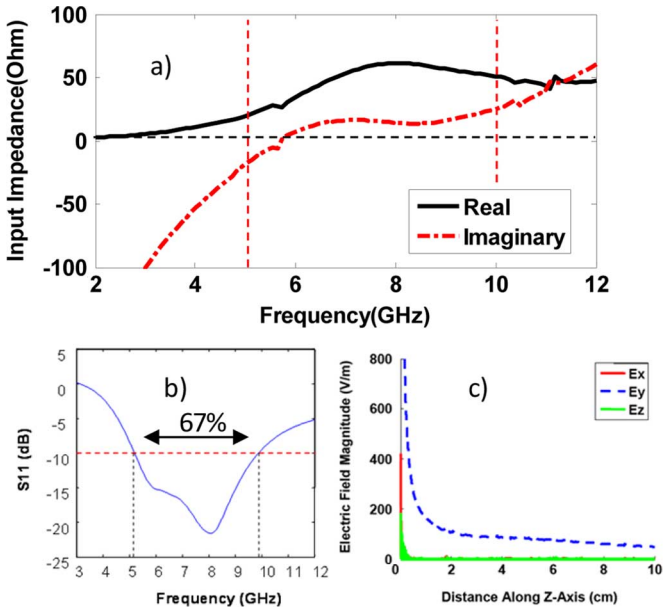

Fig. 2. (a) The input impedance and reactance of the antenna in air (b) the simulated S_{11} of the antenna referenced to 50 Ω in air and (c) the magnitude of the electric fields as a function of distance from the antenna when the y-directed port is excited (port e′e) in air.

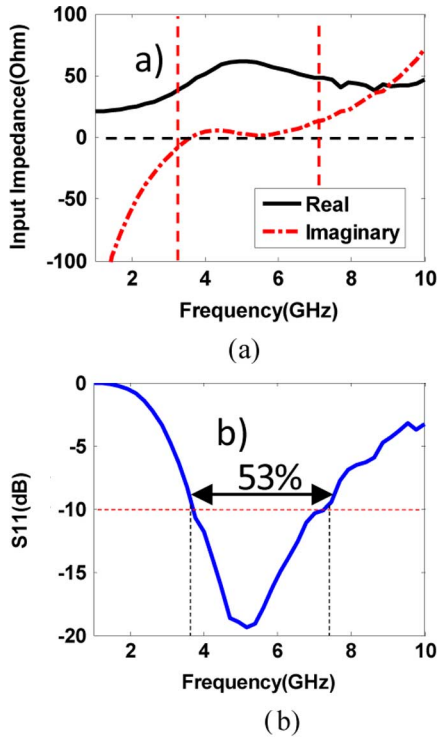

Fig. 3. (a) The simulated S_{11} of the antenna in oil and (b) the input impedance and reactance of the antenna in oil.

operates between 5–10 GHz. In addition, the antenna is capable of a dual linear polarization depending on which arms of the antenna are excited. Fig. 2(c) shows the magnitude of the electric field in each direction (x, y and z) as a function of the distance from the antenna. Fig. 2(c) shows that within millimeters of the antenna, E_y dominates as expected.

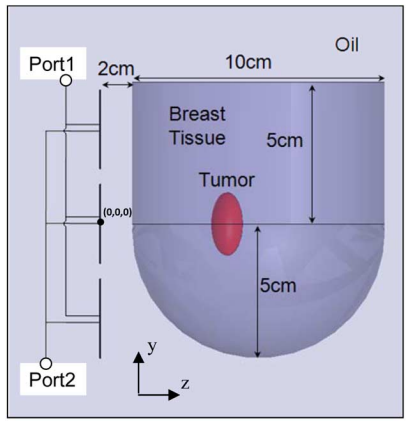

Fig. 4. The breast model with ellipsoidal tumor utilizing a three element array.

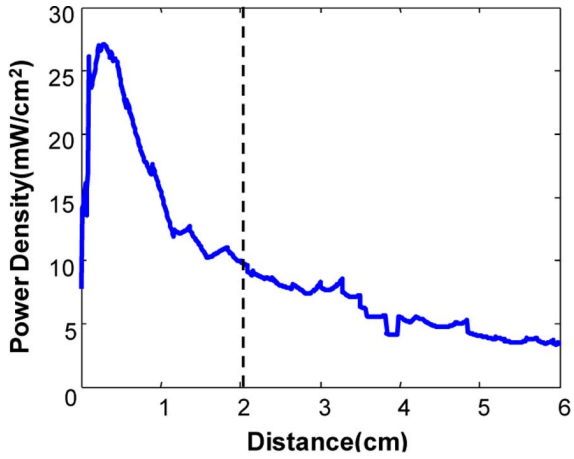

Fig. 5. Power density as a function of distance from the antenna array immersed in oil along the main beam.

A matching media is used to reduce the scattering from the breast interface. In [6] a study was conducted on various background media, with oil ($\varepsilon_r = 3$) providing the best results. For this reason, the background material is chosen to be oil for this work. This matching media affects the antennas performance slightly. The impedance and reactance in oil is shown in Fig. 3(a). The resonant band of the antenna is shifted down to 3.8–7.8 GHz corresponding to a bandwidth of 72% using a center frequency of 5.5 GHz as shown in Fig. 3(b).

To focus the beam, a three-element array is designed using the basic principles of phased arrays [7]. A beam direction of $\theta = 0^\circ$ and $\varphi = 0^\circ$ (along the z-φ) is used which is the direction of tumor location as shown in Fig. 4. This corresponds to a phase offset of 0° at the center frequency. The antennas are placed 3 cm apart measured from center to center. Two ports were defined corresponding to the horizontal and vertical polarizations of the three antenna elements as shown in Fig. 4. The vertical polarization is excited through feed points a′a and the horizontal polarization is excited through feed points e′e. The IEEE Safety Standards for exposure to electromagnetic fields mandate that, in a controlled environment, the level of electromagnetic energy in the microwave band is not to exceed 10 mW/cm^2 on human skin [8]. Fig. 5 shows the radiated power as a function of distance from the antenna when a feeding power of 100 mW is utilized. The results show that this antenna should be placed at least 2 cm away from the breast.

Due to the broadband nature of the antenna elements the distance between elements varies between $0.73\ \lambda < d < 1.43\ \lambda$. The radiation pattern of the array changes accordingly with the frequency. The

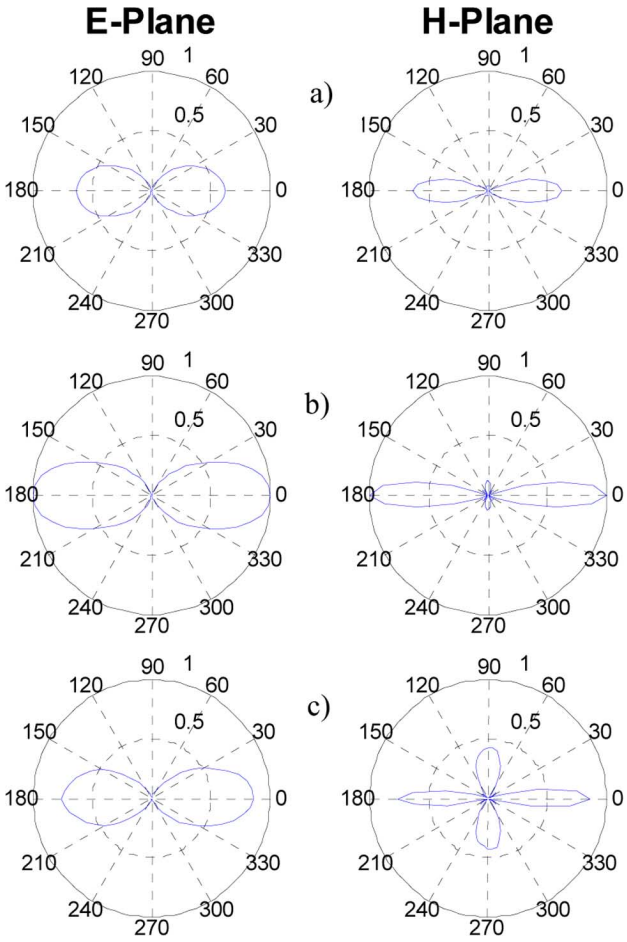

Fig. 6. Array radiation patterns at (a) 4 GHz (b) 5.5 GHz and (c) 7 GHz.

radiation pattern at 4 GHz, 5.5 GHz and 7 GHz is plotted in Fig. 6. The results show that at higher frequencies side lobes begin to form, although the main beam remains focused in the direction of the tumor where no oblique lobes are present.

III. Statistical Breast Cancer Detection

Using the Ansoft HFSS package, a simplified model of the breast is simulated as shown in Fig. 4. In the model, an ellipsoid ($a = 0.75$ cm, $b = 0.5$ cm, $c = 1.0$ cm) is used to numerically simulate a tumor. The center of the tumor is located at (0,0,6 cm) which is 6 cm from the central antenna's face along the direction of the main beam. Previous results indicated that the backscattered fields produced the best chance of statistical detection which is also used here [9]. The skin thickness is ignored in this work for comparison between results obtained using the plane waves [9]. The antenna array has two feeding ports corresponding to the vertical and horizontal polarizations. The complex S-parameters, synthetically measured at the ports, are utilized as the input of the neural network. The S-parameters at every 100 MHz are used for training and testing the network. Three tumor orientations are used with the tumor main axis 1) aligned with port 1 ($\mathrm{a}'\mathrm{a}$), 2) aligned with port 2 ($\mathrm{e}'\mathrm{e}$) and 3) oblique with 45° with regards to $\mathrm{a}'\mathrm{a}$ or $\mathrm{e}'\mathrm{e}$.

IV. Numerical Results

One hundred cases for a tumor, with the three orientations mentioned above, and one hundred cases with no tumor are simulated for a total of 400 cases. The complex relative dielectric constants of the tumor and healthy tissue are varied randomly in the ranges $9 - \mathrm{j}1 \leq \varepsilon_{\mathrm{rhealthy}} \leq 25 - \mathrm{j}6$ and $40 - \mathrm{j}10 \leq \varepsilon_{\mathrm{rtumor}} \leq 60 - \mathrm{j}30$, respectively [9]. A neural network is trained using fifty of the cases from a certain orientation and fifty cases with no tumor. The network is then tested against the remaining fifty cases from the same set. This process is repeated for each of the three orientations. The network has 82 input nodes corresponding to the complex S-parameter data at every 100 MHz in the resonant frequency band (3.8 GHz–7.8 GHz). Through experimentation, 41 hidden nodes were determined to be the optimal configuration with the network being fully interconnected. A single output node is used with an output restricted between 0 and 1.

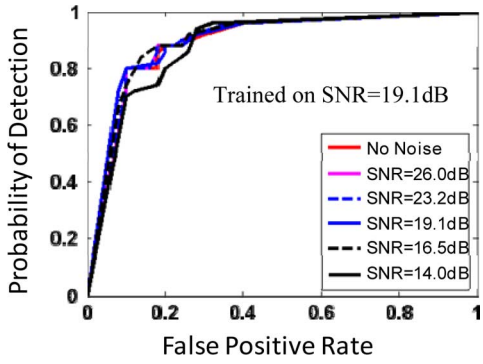

Fig. 7. ROC curve for network performance at each white noise.

White noise is added to the S-parameters based on Gaussian distribution with a mean of zero and standard deviations σ_{n}. σ_{n} is varied from 0.001 to 0.3 corresponding to a SNR of 26 dB to 14 dB. The ANN testing procedure is based on utilizing Youden's Index to determine the optimal cutoff values for the network as discussed fully in [9], [10]. Fig. 7 shows the network performance over the range of white noise and is used in determining the optimal cutoff values for the network. The number of false positives, false negatives, undecided and correct identification results are computed. Fig. 8 shows the results using a training set with noise of $\sigma_{\mathrm{n}} = 0.1$ (SNR of 19.1 dB) and a testing set with noise of $\sigma_{\mathrm{n}} = 0.2$ (SNR of 16.5 dB). Each row corresponds to a specific tumor orientation and each column corresponds to the same polarization and S-parameters. Notice that the orientation in the first row is when the tumor's main axis aligns with $\mathrm{a}'\mathrm{a}$, the second row is when the tumor's main axis is tilted 45° oblique to $\mathrm{a}'\mathrm{a}$ and the third row is when the tumor's main axis aligns with $\mathrm{e}'\mathrm{e}$. Note that in the first column of Fig. 8, port $\mathrm{a}'\mathrm{a}$ is used for excitation and for receiving. In the second column, port $\mathrm{a}'\mathrm{a}$ is used for excitation while port $\mathrm{e}'\mathrm{e}$ is used for receiving. In the third column, port $\mathrm{e}'\mathrm{e}$ is used for excitation and port $\mathrm{a}'\mathrm{a}$ is used for receiving. Finally, in the fourth column port $\mathrm{e}'\mathrm{e}$ is used for excitation and receiving. The results of Fig. 8 show that the highest percentage of correct identifications occurs when the main axis of the tumor is aligned with the excited port. For example, this ratio is 87% in the $\mathrm{S}_{11\,\mathrm{VV}}$ [see Fig. 8(a)] and $\mathrm{S}_{22\,\mathrm{HH}}$ [see Fig. 8(m)]. Notice that this percentage is decreased by 5%–7% when the main axis of the tumor is aligned with the un-excited port (90° rotation with respect to the excited port). For example, see the $\mathrm{S}_{22\,\mathrm{HH}}$ in Fig. 8(d) and $\mathrm{S}_{11\,\mathrm{VV}}$ in Fig. 8(i). The lowest detection rates of 71–76% occurred when using S_{21} or S_{12} for HV or VH [see Fig. 8(b)–(k)]. These are the cases in columns two and three.

The results of Fig. 8(d) and (i) are for the cases when the minor axis of the tumor is aligned with the excited port. If the breast was a flat surface, it is expected for these two results to be identical. The slight difference in the percentage rates in these cases can be attributed to the curvature of the breast.

Clearly, the results of Fig. 8 infer that the detection ability of the network has a correlation with the orientation of the tumor with respect to

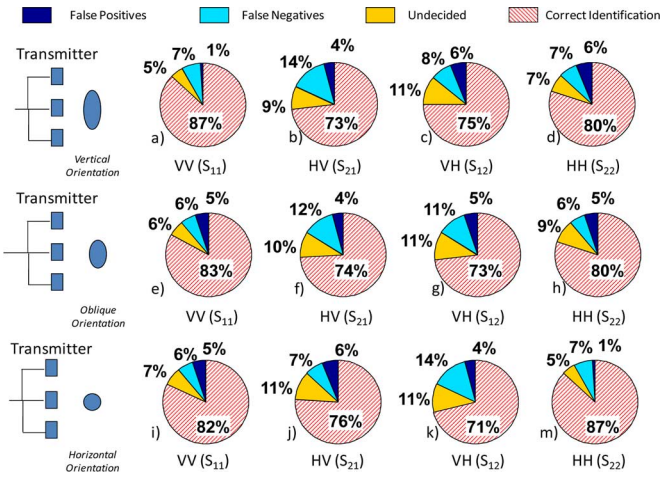

Fig. 8. Backscatter results using ANN trained on noise $\sigma_n = 0.1$ and tested versus noise $\sigma_n = 0.2$ for each tumor orientation.

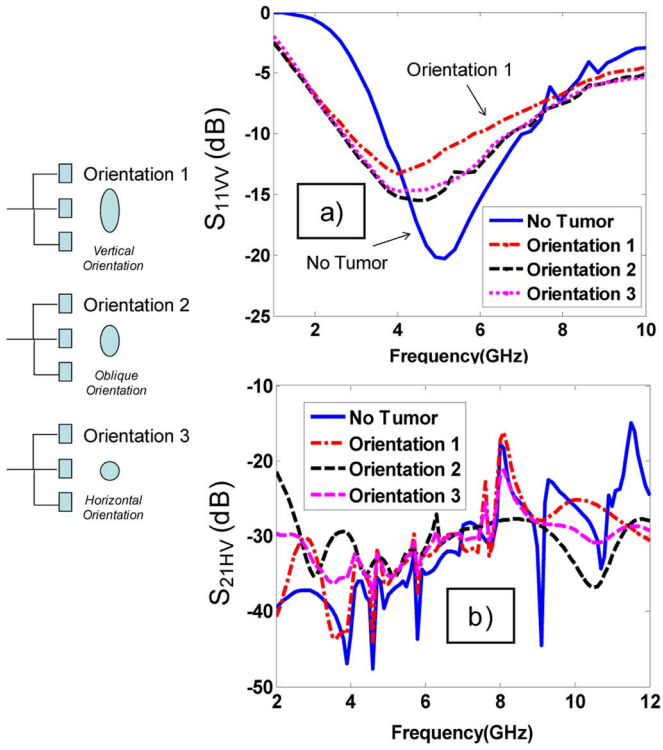

Fig. 9. Change in (a) S_{11} and (b) S_{21} due to tumor orientations in oil.

the excited polarization. To clarify this point even more, the S_{11} and S_{21} parameter is plotted for all tumor orientations in Fig. 9 when port a′a is excited. The results of Fig. 9(a) show that the largest difference of around 6 dB exists between the S_{11} when no tumor is present and the S_{11} when the tumor is aligned with the excited port a′a (orientation 1). This larger difference is more detectable to the ANN which is consistent at all frequencies in the resonant band as shown in Fig. 9(a). On the other hand, the smallest difference of the S_{11} exists with orientation 3 when the minor axis of the tumor is aligned with the excited port a′a [see Fig. 8(i)]. The difference for the oblique orientation is almost in the middle of these two cases [see Fig. 8(e)]. Fig. 9(b) demonstrates the signals collected in the cross-polarized HV case with insignificant difference with the presence of a tumor. This leads to a reduction in tumor detection efficiency as seen in the second and third columns of Fig. 8. This confirms the statistical results shown in Fig. 8 and also the results reported in [11].

Many factors such as tumor size, position, and other scattering objects must be considered in detection algorithms. As an example, using an increased number of simulations for training the network has shown to improve network performance. In [9] 14 000 cases were simulated when plane waves and a point receiver was used for excitation and receiving respectively. A two region model and multiple random tumor locations were investigated in [9]. In this work 400 total cases with a single tumor location were simulated due to the greatly increased CPU time requirements for the 3D model shown in Fig. 4. Each simulation in [9] required approximately 2–3 minutes on a SUN Opteron Server, while in this work each simulation required 2–3 hours on a Dell AMD Desktop where the Ansoft package is available. The effect of random tumor locations has shown to not degrade the network performance [9].

A model based on a patient's MRI scan is developed to study the effect of the skin, a heterogeneous breast medium and the low contrast values reported in [2] as published in [12]. By varying the amount of fibro-glandular content in the breast the signature of the tumor is shown to reduce to 1 dB compared with 6 dB shown in Fig. 9(a), [12]. The results require processing times of 15–20 hours compared to 2–3 hours in the current model. As the tumor signature decreases, however, the network performance is expected to degrade correspondingly and is the subject of further research.

V. Conclusion

In this work a broadband planar antenna is designed with a dual linear polarization. This antenna consists of two perpendicular dipole-like antennas; one is vertical and one is horizontal. Using this dual polarized antenna allowed the calculation of all vertical and horizontal co- and cross-polarizations. The effect of the polarization is investigated and shown to have an influence on the statistical detection using the ANN. The highest detection rate was shown to occur when the tumor's main axis is aligned with the excited polarization. The results in this work show the importance of collecting data at all polarizations since the orientation of a real breast tumor is unknown. By rotating the antenna the likelihood of using a polarization parallel to the tumors main axis is augmented and this will subsequently increase the percentage of correct identifications of breast tumors.

Ongoing work is being conducted to integrate the designed antenna with a MEMS rotatable platform to scan the breast to increase the likelihood of tumor detection.

References

[1] A. M. Campbell and D. V. Land, "Dielectric properties of female human breast tissue measured in vitro at 3.2 GHz," *Phys. Med. Biol.*, vol. 37, pp. 193–210, Jan. 1992.

[2] M. Lazebnik, D. Popovic, L. McCartney, C. B. Watkins, M. J. Lindstrom, J. Harter, S. Sewall, T. Ogilvie, A. Magliocco, T. M. Breslin, W. Temple, D. Mew, J. H. Booske, M. Okoniewski, and S. C. Hagness, "A large-scale study of the ultrawideband microwave dielectric properties of normal, benign, and malignant breast tissues obtained from cancer surgeries," *Phys. Med. Biol.*, vol. 52, pp. 6093–6115, 2007.

[3] C. Rappaport, "A Dispersive microwave model for human breast tissue suitable for FDTD computation," *IEEE Antennas Wireless Propag. Lett.*, vol. 6, 2007.

[4] M. El-Shenawee and E. Miller, "Spherical harmonics microwave algorithm for shape and location reconstruction of breast cancer tumor," *IEEE Trans. Med. Imaging*, vol. 25, pp. 1258–1271, Oct. 2006.

[5] S. Suh, "A comprehensive investigation of new planar wideband antennas," Ph.D. dissertation, Virginia Polytechnic Institute, Blacksburg, VA, USA, 2002.

[6] J. M. Sill and E. C. Fear, "Tissue sensing adaptive radar for breast cancer detection: Study of immersion liquids," *Electron. Lett.*, vol. 41, pp. 113–115, Feb. 2005.

[7] W. L. Stutzman and G. A. Thiele, *Antenna Theory and Design*, 2nd ed. New York: Wiley, 1997.
[8] *IEEE International Committee on Electromagnetic Safety (SCC39)*, IEEE Std C95.1, Apr. 19, 2006, IEEE standard for safety levels with respect to human exposure to radio frequency electromagnetic fields, 3 kHz to 300 GHz.
[9] D. A. Woten, J. Lusth, and M. El-Shenawee, "Interpreting artificial neural networks for microwave detection of breast cancer," *IEEE Microw. Wireless Comp.*, to be published.
[10] D. Woten, "Artificial neural networks for breast cancer detection using micro antennas," M.S. thesis, Univ. Arkansas, Fayetteville, AR, 2007.
[11] X. Yun, E. C. Fear, and R. H. Johnston, "Compact antenna for radar-based breast cancer detection," *IEEE Trans. Antennas Propog.*, vol. 53, pp. 2374–2380, Aug. 2005.
[12] D. Woten, S. Pandalraju, and M. El-Shenawee, "Breast skin effect on scattered electromagnetic fields," in *Proc. Appl. Comput. Electromagn. Symp.*, Mar. 2008, pp. 80–85.

Accurate Analysis of Meanderline Polarizers With Finite Thicknesses Using Mode Matching

Kwok Kee Chan, Teng Wah Ang, Tan Huat Chio, and Tat Soon Yeo

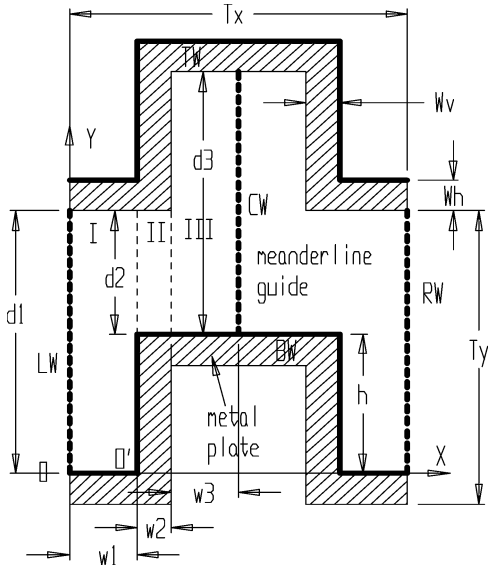

Fig. 1. Unit cell of a meanderline polarizer.

***Abstract*—Most of the existing methods for the analysis of meanderline polarizer assume that the embedded metallic grids are infinitely thin. A modal procedure is presented here for treating meanderline grids with finite thicknesses. The space between the metallic grids in a unit cell is considered as a meanderline waveguide with a stepped cross-section and length given by the grid thickness. The modes of this guide are obtained using the transverse resonance technique. A generalized scattering matrix characterization of the grid is obtained by field matching of the modes of the meanderline guide and the free space Floquet guide. The accuracy of this approach is verified by the very good agreement obtained between predicted and measured transmission phases of polarizer grids.**

***Index Terms*—Circular polarization, generalized scattering matrix, mode matching methods, printed circuits.**

I. Introduction

The 90° meanderline polarizer is a very useful external means for converting an incident linear polarized plane wave into a circular polarized wave. The polarizing grid is doubly periodic and its configuration in a unit cell is shown in Fig. 1. In the following development, we will deal with a grid under normal incidence where the incident wave has its electric vector oriented in the 45° plane. This incident wave may be resolved into the two component TE_{00} and TM_{00} waves. For the former, the grid is normal to its electric vector and therefore appears to be capacitive. For the latter, the grid is parallel to the electric vector and hence is inductive to the incident wave. With the appropriate parameters and number of grid layers, a 90° phase differential can be created and approximately maintained between the TE_{00} and TM_{00} waves over a very broadband.

Manuscript received October 24, 2007; revised June 28, 2008. Current version published November 14, 2008.

K. K. Chan is with the Chan Technologies Inc., Brampton, ON L6Y 5H1, Canada (e-mail: kwok-kee.chan@rogers.com).
T. W. Ang and T. H. Chio are with the DSO National Laboratories, Singapore 118230, Singapore.
T. S. Yeo is with the Temasek Defence Science Institute, Singapore 117576, Singapore.

Color versions of one or more of the figures in this paper are available online at http://ieeexplore.ieee.org.
Digital Object Identifier 10.1109/TAP.2008.2005548

The existing methods for the analysis and design of the meanderline polarizer may be classified into two groups. The first group [1] makes use of equivalent network models of the grids and dielectric layers as well as transmission line theory to predict the polarizer performance. A number of iterations consisting of model adjustments, fabrication and test are required to arrive at a satisfactory design. The second group [2]–[4] makes use of the Floquet Mode expansion MoM to solve for the currents on the metallic grids to give the scattered fields. An integral equation of the grid currents is formulated by enforcing the continuity of the electric fields and discontinuity of the magnetic fields caused by the currents. In both groups, the metallic grid is assumed to be infinitely thin, which is essential for the second group. If the metallization is electrically thick, for instance, in a free-standing grid or operating at the higher frequencies or resulting from the use of heavy metal cladding, the measured electrical performance obtained will be in error relative to the prediction. This is typically manifested as a frequency shift of the electrical response. Scattering of finite thickness plates perforated by circular and rectangular apertures [5] and by arbitrary apertures [6] have been analyzed using the method of moments (MoM). No work on thick polarizer grids has yet been reported. To account for the thickness of the polarizer grids, we propose to use the mode matching method [7], [8] to solve the scattering problem. The fields in between the grids, rather than the grid currents are utilized to describe the grid scattering. This modelling approach has the advantage of using much fewer Floquet modes in the field expansion. It also allows various conductor widths to be used and they are no longer required to be narrow.

As shown in Fig. 1, the space in between two parallel grids in a unit cell is labelled here as a meanderline guide (MLG). Under normal incidence, the guide is symmetric about the centre wall (CW). The top (TW) and bottom (BW) walls of the guide are perfect electric conductors (PEC). Under normal TE incidence, the left (LW) and right (RW) walls as well as CW are perfect magnetic conductors (PMC). Under normal TM incidence, LW, RW and CW are PEC walls. For the MLG with magnetic sidewalls, we need to find the TEM, TE and TM modes. For the MLG with electric sidewalls, TE and TM modes need to be determined. These modes are found using the transverse resonance technique. Field matching between the MLG modes and the Floquet modes